Ecosystems
https://doi.org/10.1007/s10021-025-00992-7

ECOSYSTEMS

ORIGINAL ARTICLE

A Negative Fire–Vegetation Feedback Substantially Limits Reburn Extent Across the North American Boreal Biome

Alan J. Tepley,[1,2]* Xianli Wang,[2] Mike D. Flannigan,[3] and Marc-André Parisien[2]

[1]*Department of Forestry, Fire, and Rangeland Management, California State Polytechnic University, Humboldt, Arcata, California, USA;* [2]*Canadian Forest Service, Natural Resources Canada, Northern Forestry Centre, Edmonton, Alberta, Canada;* [3]*Thompson Rivers University, Kamloops, British Columbia, Canada*

Highlights

- A negative fire–vegetation feedback reduced reburn extent by 5 Mha over 33 years
- Resistance to reburning was strongest in the most fire-prone areas
- This resistance will likely continue to dampen climate change impacts on wildfire

Abstract

The North American boreal biome (NAB) is warming at 2–4 times the mean global rate, contributing to increasing wildfire activity. The degree to which this trend alters biome-level feedbacks to global climate depends on how strongly bottom-up feedbacks between fire and vegetation dampen the effects of climate drivers. As young vegetation recovering from fire covers a growing portion of the landscape, it could resist reburning, buffering against further increases in fire. Resistance to reburning could be particularly strong in the NAB, where slow post-fire fuel accumulation is sometimes combined with a fire-driven shift from conifers toward less-flammable, deciduous trees. However, continued warming could eventually override the feedback. To quantify the strength of the feedback throughout the biome, we divided the NAB into 27 Fire Regime Units (FRUs) and used fire data from 1986 to 2018 to determine the area expected to have burned more than once (that is, reburned) within each FRU under the null assumption that recent fire does not influence burn probability. Then, we ran a spatial simulation to quantify the strength of departure from the null

Received 6 March 2025; accepted 9 July 2025

Supplementary Information: The online version contains supplementary material available at https://doi.org/10.1007/s10021-025-00992-7.

Author Contributions: AJT, MAP, XW, and MDF conceived and designed the study. AJT performed research. AJT analyzed data. AJT contributed new methods or models. AJT, MAP, XW, and MDF wrote the paper.

*Corresponding author; e-mail: alan.tepley@humboldt.edu

Published online: 18 September 2025

value while accounting for variation driven by stochastic fire patterns. Reburn extent was 5 Mha less than expected without the feedback. Departure from the null model was strongest in the most fire-prone FRUs, suggesting that the feedback will continue to dampen climate-driven increases in wildfire activity. These results provide a sound baseline from which to identify potential weakening of the feedback under continued warming, and our approach could be expanded to other biomes.

Key words: fire–vegetation feedback; reburn; null model; boreal forest; wildfire; analytical model; spatial simulation; neutral landscape.

Introduction

The boreal forest biome accounts for approximately one-third of both the global forested area and terrestrial carbon stocks (Pan and others 2011; Brandt and others 2013). Climate change has driven an increase in wildfire activity across the biome in recent decades (Hanes and others 2019; Burrell and others 2022). This trend of increasing wildfire activity has the potential to alter biome-level feedbacks to global climate, depending on the degree to which the increase in wildfire activity alters forest cover, species composition, and soil carbon pools (Archibald and others 2018). Climate-driven changes to boreal fire regimes were most evident in Canada's 2023 fire season, when May–October temperatures were 2.2°C above the 30-year mean and almost 15 million hectares burned, making it Canada's largest fire year on record (Boulanger and others 2024; Jain and others 2024). The probability of similarly large fire years will increase in a warming climate (Kirchmeier-Young and others 2024), and the fire-driven release of carbon from above- and belowground stores could accelerate climate warming (Walker and others 2019; Phillips and others 2022).

Predicting the degree to which climate change will alter boreal biome-level feedbacks to the climate system requires an understanding of how the bottom-up feedbacks between fire and vegetation will moderate the effects of top-down climate drivers. The top-down drivers of increasing wildfire are particularly pronounced in boreal regions, which have been warming at 2–4 times the mean global rate over recent decades (Zhang and others 2019; Rantanen and others 2022). The resulting feedbacks to global climate (Archibald and others 2018) are likely to be more prominent in North American than Eurasian boreal forests because wildfires in North America tend to be larger and more severe (Wooster and Zhang 2004; de Groot and others 2013; Rogers and others 2015). However, the North American boreal forest (hereafter, NAB) may have particularly strong bottom-up feedbacks that could dampen the impacts of these top-down changes.

As the trend of rapid warming continues to drive increasing wildfire activity across the NAB, a growing portion of the landscape will be covered by young vegetation, which may be resistant to burning for a period of years to decades (Héon and others 2014; Hart and others 2019). The primary mechanisms underlying this resistance to reburning (that is, the negative fire–vegetation feedback) are the slow fuel buildup following high-severity fire (Thompson and others 2017; Walker and others 2020), sometimes combined with an increase in the abundance of less flammable, broadleaf deciduous trees after the burning of conifer-dominated forests (Johnstone and others 2010; Whitman and others 2018). Because the accumulation of flammable fuel is particularly slow following fire in the NAB, it may have a stronger negative fire–vegetation feedback than found in most regions globally. Fuel buildup is particularly slow in wetlands (Johnston and others 2015), which are much more widespread in the NAB than most other temperate forest regions (Brandt 2009), further strengthening the potential for the negative fire–vegetation feedback to moderate the climate-driven increases in wildfire activity.

A negative fire–vegetation feedback has also been suggested to limit short-interval reburns in portions of the western United States (Parks and others 2015, 2018), but the duration of this feedback may be short (for example, < 10 years) due to rapid fine fuel accumulation (Buma and others 2020). It was predicted to play only a minor role in dampening future climate-driven increases in fire extent across the western United States (Abatzoglou and others 2021). By contrast, the negative feedback in the NAB was interpreted to have substantially limited wildfire activity in the past (Héon and others 2014; Erni and others 2017; Hoecker and Higuera 2019), and simulation models suggest potential to offset much of the effect of climate warming on future wildfire activity (Boulanger and others 2017; Marchal and others 2019; Foster and others 2022).

Despite empirical evidence of a negative fire–vegetation feedback in portions of the NAB and models projecting its role in dampening the effect of climate on future wildfire activity, a systematic

approach to quantifying contemporary variation in the strength of the fire–vegetation across the NAB is lacking. A stronger baseline understanding of how the fire–vegetation feedback has moderated wildfire activity in recent decades is needed to strengthen projections of future wildfire trends and feedbacks of the NAB to global climate. For instance, as the climate continues to warm and severe fire weather becomes more common (Jain and others 2022), there is increasing potential to override the resistance to reburning (Buma and others 2022; Whitman and others 2024). Then again, increases in fire frequency and/or severity could reduce soil organic matter (Walker and others 2019), thereby favoring post-fire regeneration of deciduous trees over conifers, as documented in northwestern portions of the NAB in recent decades (Johnstone and others 2020; Baltzer and others 2021; Massey and others 2023). The resulting expansion of forests dominated by less flammable, deciduous species might maintain or strengthen the feedback, even in the face of drier fuels and a greater frequency of severe fire weather (Mack et al. 2021).

Here, we develop a combined analytical and simulation modeling approach to quantify the variation in the strength of the fire–vegetation feedback across the NAB over recent decades (from 1986 to 2018). We address two main questions: (1) How strong is the resistance to reburning across the NAB? and (2) To what degree does the strength of that resistance vary geographically? By addressing these questions, we will develop a sound baseline for understanding the degree to which the feedback could limit further climate-driven increases in wildfire activity. This baseline understanding will also help to identify if or when we begin to see a weakening of the feedback in the face of drier fuels and an increasing frequency of severe fire weather, or if there is a strengthening of the feedback in response to increasing deciduous forest cover in portions of the NAB.

Methods

Study Area

The North American boreal biome (NAB) spans about 600 million ha, with forest and woodland comprising almost 60% of that area (Brandt 2009). Lakes, wetlands, and meadows account for most of the remaining area. Conifers typically dominate long-unburned stands, but broadleaf deciduous species may be abundant at lower latitudes and soon after fire in portions of the biome (Johnstone and others 2011; Shenoy and others 2011; Hoecker and Higuera 2019). The dominant conifers are white spruce (*Picea glauca* (Moench) Voss), black spruce (*Picea mariana* (Mill.) Britton, Sterns & Poggenb.), balsam fir (*Abies balsamea* (L.) Mill.), jack pine (*Pinus banksiana* Lamb.), and tamarack (*Larix laricina* (Du Roi) K. Koch). Major broadleaf tree species include trembling aspen (*Populus tremuloides* Michx.), balsam poplar (*P. balsamifera* L.), and birches (*Betula papyrifera* Marshall and *B. neoalaskana* Sarg.). The NAB has a sparse human population compared to most forested regions globally. Human land use—primarily urban development, forest harvesting, agriculture, and mining—is concentrated primarily along the southern part of the biome. These activities have altered wildfire frequency, seasonality, and size, with the strength of that influence decreasing with distance from the more populated areas (Tymstra and others 2020; Parisien and others 2023).

To evaluate spatial variation in the resistance to reburning, we divided the NAB into 27 smaller regions, hereafter referred to as Fire Regime Units (FRUs; Figure 1a), following a recent classification of fire regimes across Canada (Erni and others 2020). The FRUs of Canada were identified using 1970–2016 datasets for five fire regime metrics: fire frequency (number of fires per unit area per unit time), burn rate (proportion of area burned per year), fire size, ignition source, and seasonality. These variables indirectly account for much of the underlying variation in macroclimate, topography, soils, vegetation, and ignitions that drive variation in fire regimes.

For Canada, we included the FRUs located within the boreal forest region of Brandt (2009), excluding FRUs 20 and 30, which are currently dominated by agricultural land use, and FRUs 43 and 46, which are composed largely of rocky ridges that lack continuous flammable vegetation. We also merged five of the smaller FRUs with their neighboring FRU to maintain a narrower range of sizes of our analysis units. For Alaska, we limited our analysis to the following Level III Ecoregions of the U. S. Environmental Protection Agency (2013): Interior Forested Lowlands and Uplands (3.1.1), Interior Bottomlands (3.1.2), Yukon Flats (3.1.3), Ogilvie Mountains (3.2.1), and Interior Highlands (6.1.1). These ecoregions include 93% of the total area burned in Alaska between 1986 and 2018. Because the boreal ecoregions of interior Alaska form a mosaic, where non-contiguous patches of two ecoregions are embedded within the others, we combined the five ecoregions into one region. We labeled this region FRU AK, for consistency

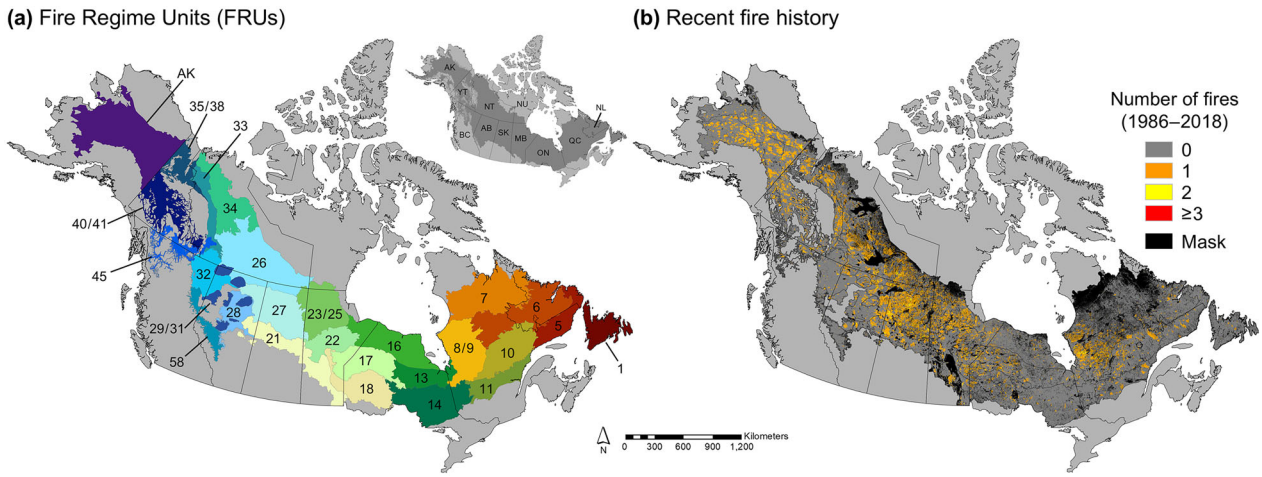

Figure 1. Illustration of **a** the 26 Fire Regime Units (FRUs) of Canada plus the boreal forest area of Alaska, representing the full extent of the North American boreal forest biome. The FRU numbers shown on the map correspond to their identification numbers used throughout the text and in Table 1. Fire regime statistics of the FRUs are summarized in Appendix S1. In **b**, the area that burned between 1986 and 2018 is color-coded by the number of times each 1-ha pixel burned over that period. Masked areas include water bodies, urban and built-up land cover, cropland, tundra, and exposed rocky ridges. The inset map depicts the extent of the North American boreal forest (Brandt 2009; gray shading) in relation to the boundaries of Alaska (AK) and the Canadian provinces and territories: AB = Alberta, BC = British Columbia, MB = Manitoba, NL = Newfoundland and Labrador, NT = Northwest Territories, NU = Nunavut, ON = Ontario, QC = Québec, SK = Saskatchewan, and YT = Yukon Territories.

with the terminology used to name the subdivisions of the boreal forest within Canada (Figure 1a). Fire regime statistics for the 27 FRUs are provided in Appendix S1.

Modeling Approach

To determine whether resistance to reburning is evident in the contemporary fire record (1986–2018), and if so, to compare the strength of that resistance across the NAB, we first produced a null model for each FRU. The null model quantifies the area expected to have burned more than once (that is, reburned) between 1986 and 2018 under the null hypothesis that the probability of burning in each year is independent of previous fires (that is, that fire-driven changes to vegetation, fuel, and microclimate have no influence on subsequent fire occurrence).

We began by producing the null model analytically, using the time series of annual area burned across the FRU, as explained under the '*Analytical model*' heading below. To assess the strength of the difference between the null and observed reburn area, we had to know the degree to which stochastic variation in annual burn patterns could drive variation in the area that reburns under the null model. We quantified this stochastic variation by running a spatial simulation where the area that burned each year followed the observed fire record, but the burn patterns in each year were independent of the time since previous fires, as explained under the '*Simulation model*' heading. After numerous replicates, we generated a frequency distribution of the area expected to have reburned under the null model. From this distribution, we assessed the likelihood that the observed reburn extent could have occurred in a system with no feedbacks.

Fire and Mask Datasets

Annual fire perimeters were acquired from the National Burned Area Composite (NBAC; Hall and others 2020; https://cwfis.cfs.nrcan.gc.ca/datamart/metadata/nbac) for Canada and the Monitoring Trends in Burn Severity project (MTBS; Eidenshink and others 2007; https://www.mtbs.gov/) for Alaska. The Canadian NBAC dataset was developed, in part, to provide an accurate and consistent method for removing unburned patches and water bodies from within fire perimeters (Skakun and others 2022), thereby improving estimates of annual area burned. For the MTBS perimeters, we used the entire area within each fire perimeter, even though it may include small patches within the 'unburned to low' burn-severity class. This class may include pixels that experienced a low-severity or sub-canopy burn, pixels with a mix of burned and unburned vegetation, or truly unburned pix-

els, including water bodies and areas of bare rock, which we masked out, as described below. We limited our analysis to fires larger than 200 ha, which accounted for 97% of the area burned across Canada in the second half of the twentieth century (Stocks and others 2002). We converted the fire polygons to raster of 100-m resolution, and we masked out all non-flammable land cover (Figure 1b).

To generate the mask layer for Canada, we used the water, urban, tundra, and non-fuel classes of the 2019 fuel types layer of the Fire Behavior Prediction (FBP) System (updated from Beaudoin and others 2014; https://cwfis.cfs.nrcan.gc.ca/background/maps/fbpft). The 'non-fuel' category includes cropland and rocky ridges. It also includes recently burned areas, which are initially represented as non-fuel and expected to revert to other fuel types as the vegetation regrows. Because treating recently burned areas as non-fuel is inconsistent with our null model, we filtered this class to include only those portions of the non-fuel class that have not burned since at least 1986. This step enabled us to mask out cropland and persistent non-burnable areas (for example, rocky ridges) while retaining recently burned areas. For Alaska, we developed the mask using the 2015 land-cover data of the North American Land Change Monitoring System (http://www.cec.org/north-american-land-change-monitoring-system/), which was derived from Landsat imagery at 30-m resolution. We masked out six of the 19 land-cover classes to remove water, persistent snow and ice, tundra, cropland, and barren land cover (classes, 11, 12, 15, 16, 17, and 18). Across all 27 FRUs, masking to exclude non-burnable land cover reduced the analysis area by 23%, from 5.2 to 4.0 million km^2 (Figure 1b).

We resampled both mask layers to 100-m resolution and calculated the time series of annual area burned within each FRU as the area burned by each fire larger than 200 ha (or 400 ha in Alaska) within the unmasked land area. Although the fire perimeters were generated primarily from 30-m Landsat data, we used 100-m resolution raster for our analyses as a compromise between the Landsat data and the 250-m resolution of the primary dataset used for masking out non-burnable areas (the FBP fuel types layer). Also, with a focus on the number of fires over time, the difference between 30- and 100-m resolution was likely to have little influence on our results. In tests on a subset of FRUs, the reburn extent differed by less than 0.02% when calculated using 100-m raster compared to the polygon fire perimeters. Since we conducted the analysis for each FRU individually, we analyzed fires that crossed the Canada–Alaska border by selecting only the portion of the fire that fell within the target FRU, using the dataset developed for the respective country.

Analytical Model

To analytically construct a null model of the proportion of each FRU expected to have burned a given number of times (n) in the absence of fire–vegetation feedbacks, we modeled the number of fires occurring in an arbitrarily small pixel (ca. 1 ha) over time as the number of successes (burns) in t independent, non-identical Bernoulli trials, where t is the number of years in the observed fire record (1986–2018 equals 33 years). The null assumption that the probability of burning in any year is unaffected by previous fires enabled us to treat the probability of burning in each year as an independent trial. This null assumption then enabled us to view year-to-year variation in area burned as driven by top-down processes (for example, climate or weather), which, in turn, made the Bernoulli trials non-identical—the probability of success (burning) varied across the independent trials (years), but not as a function of time since the previous fire.

The number of successes (burns) in t independent, non-identical trials follows the Poisson binomial distribution (Hong 2013),

$$P\{N(t) = n\} = \sum_{B \in Y_n} \prod_{i \in B} p_i \prod_{j \in B^c} (1 - p_j) \qquad (1)$$

where $N(t)$ is the number of times a pixel burns in t years, and Y_n represents all subsets of n years that can be drawn from the years in the analysis. For each realization, B is the subset of years in which the pixel burns, and B^c (the complement of B) is the subset of years when it does not burn. The probability that the pixel burns in the ith year is p_i, which we set equal to the proportion of the FRU observed to have burned in the corresponding year (after masking out non-burnable land cover). For instance, if 5% of the FRU burned in a particular year and we were to randomly select one pixel within the FRU, the probability that the selected pixel burned that year is 0.05. Similarly, $1 - p_j$ represents the probability that a pixel did not burn in the jth year, which we set equal to the proportion of the FRU that did not burn in the corresponding year of the observed record.

We can easily apply Eq. (1) to determine the probability that a pixel remains unburned over t years. In this case, B would be empty, and the

equation simplifies to the product of the probabilities of not burning in each year ($(1-p_1) \times (1-p_2) \times \ldots \times (1-p_t)$, where p_1 is the proportion of the landscape that burned 1986, p_2 is the proportion burned in 1987, etc.). To calculate the probability of burning one or more times ($P\{N(t) \geq 1\}$), we first generated a set (Y_n) of all possible combinations of n years in which the pixel could burn. Then, we iteratively selected each subset of burned years (B) and calculated the product of the probabilities of burning (p_i) during each of those years. We then multiplied this value by the product of the probabilities of not burning ($1-p_j$) in each of the remaining years given in B^c. Finally, we summed these values over all possible subsets of n years.

As n increases, the set of possible years in which a pixel could burn increases rapidly, following $Y_n = t!/(n! \times (t-n)!)$ (Ross 2010). Thus, with $t = 33$ years, there are 528 possible combinations of 2 years in which a pixel could burn, 5456 combinations of 3 years, and 40,920 combinations of 4 years. There are methods to approximate the Poisson binomial distribution when either n or t is large (Hong 2013). However, our time series is short enough that we could make the calculations directly. We also verified our calculations by recognizing that the probability of burning two or more times, $P\{N(t) \geq 2\}$ (that is, the probability of reburning), is equal to $1-P\{N(t) = 0\}-P\{N(t) = 1\}$.

If we assume that fire regimes are spatially homogeneous within the unmasked portion of each FRU, the probability of a pixel burning n times over the t-year analysis also represents the proportion of the FRU expected to have burned n times in t years under our null model. Thus, we used Eq. (1) to calculate the proportion of each FRU expected to have burned any number of times over the analysis period. Then, we compared these values to the proportion of each FRU observed to have burned the corresponding number of times.

Spatial Simulation

Although Eq. (1) enables us to determine whether the observed reburn area is more or less than expected under the null model, it does not tell us whether this difference exceeds the variance expected due to stochastic variation in annual fire patterns. To assess the degree to which stochastic variation could influence the reburn area found in a single realization under the null hypothesis, we conducted a spatial simulation on a neutral landscape (Gardner 2017). In each replicate, we randomly generated fires year-by-year, where the proportion of the landscape that burns each year follows the proportion burned in the corresponding year of the observed record, and we simulated each year's fires independent of previous years (Figure 2a).

For each year, we simulated fires on a 10^6-cell grid (1000 × 1000 cells). Because we simulated fires on a neutral landscape, we did not simulate fire spread per se. Instead, we generated clumps of cells to represent burned patches, where we calibrated the size of the clumps based on the observed fire-size distribution across the FRU. This approach speeds up the simulation process and required few assumptions or parameters to calibrate. After simulating each year's fires, we summed the grids over t years to determine the number of times each cell burned over a single replicate. We repeated this process 1000 times ($t = 33$ years per replicate) to generate a distribution of the proportion of the FRU that reburned per replicate. From these distributions, we assessed the probability that the observed reburn area could have occurred under the null model with no feedbacks.

Our process for simulating fires during each year of the simulation involved first producing a Gaussian random field using package 'NLMR' (Sciaini and others 2018) in R version 4.4.3 (R Core Team 2025). The resulting cell values varied continuously from 0 to 1. To convert these to a binary grid representing burned and unburned cells, we set a threshold, above which cells were burned, and below which they remained unburned (values of 1 and 0, respectively). We set the threshold so that each cell burned with probability p_i in the ith year of each replicate. As in Eq. (1), p_i is equal to the proportion of the landscape observed to have burned in the corresponding year (Figure 2a). To simulate this probability of burning, we first generated a unique series of g Bernoulli random numbers for each year of the simulation, where g is the total number of cells in the grid (10^6), and p_i provides the probability of success (burns) in the random numbers. Then, we set the threshold so that the proportion of the grid that burns is equal to the proportion of successes across the Bernoulli random numbers. Setting the threshold in this manner produces stochastic variation in the area that burns per year, but as the number of replicates increases, the mean proportion of cells that burn in the ith year approaches p_i.

The key parameter that we calibrated when generating the Gaussian random fields was the scale of spatial autocorrelation, which determines the distribution of simulated patch sizes. We refer to the patch-size distribution rather than the fire-size distribution because an individual fire could be

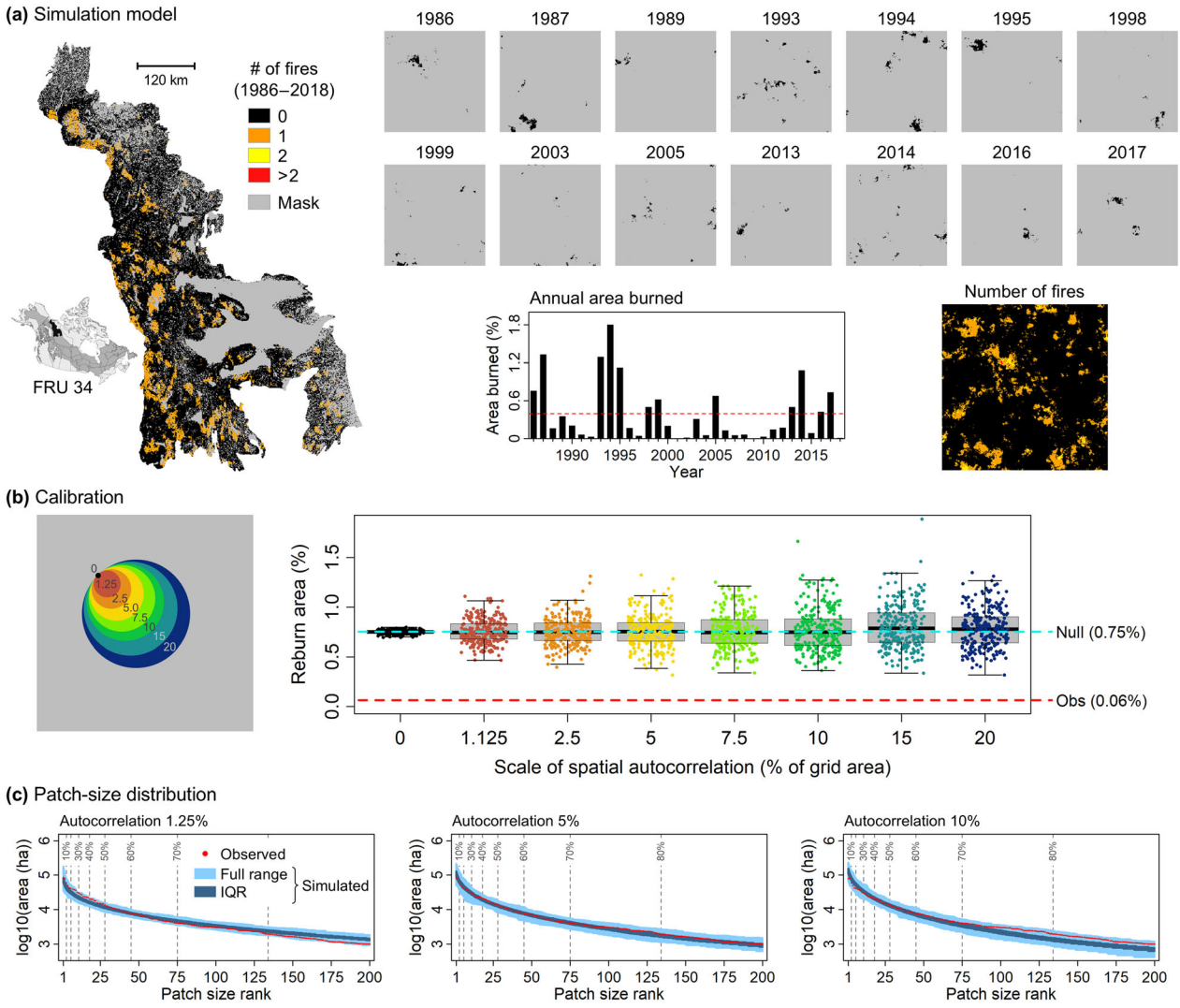

Figure 2. Illustration of the application and calibration of the null simulation model. In **a**, the observed fire pattern (left) is shown along with a bar chart of the annual area burned (bottom center). Wildfires were simulated annually, where the proportion of the grid that burns each year is based on the proportion of the landscape burned in the corresponding year in the bar chart, and fire patterns are independent of areas burned in previous years. Simulated fires for the 14 largest fire years (accounting for 87% of the total area burned in the FRU) are shown in the upper part of **a**, where burned cells (black) have a value of 1, and unburned cells (gray) have a value of 0. At the end of each replicate, the annual grids are summed to provide the number of fires per cell, as shown in the lower right of panel (**a**). Although the mean reburn area across numerous replicates is equal to the value determined by Eq. (1), the variance around that value increases as the simulated fire sizes increase, as shown in (**b**). We controlled the simulated fire sizes by adjusting the scale of spatial autocorrelation, as specified by entering the range of the variogram in NLMR (Sciaini and others 2018). To facilitate interpretation, we represent the scale of spatial autocorrelation as the percentage of the grid area covered by a circle with a radius equal to the range of the variogram. Results of 250 replicates at eight scales of spatial autocorrelation are shown as points overlaid on box-and-whisker plots to illustrate how the variance across replicates increases with the scale of spatial autocorrelation. We adjusted the autocorrelation parameter until we reached the closest correspondence between the simulated and observed patch-size distribution. Panel, **c** shows results of 500 replicates each at three scales of spatial autocorrelation, where we selected a scale of 5% of the grid area (center panel) for this FRU. To plot the patch-size distributions, we ranked all patches over the 33-year analysis from large to small. Dashed vertical lines represent the patch size that accounts for a given percentage of the observed area burned over the full analysis period. Light and dark blue shading represent the full range and interquartile range (IQR) of patch sizes for the corresponding rank across the different replicates.

split along an FRU boundary, or it could be divided into two or more non-contiguous patches by masked cells (for example, water bodies or rocky ridges) within the FRU. We specified the scale of spatial autocorrelation by setting the range of the underlying variogram (Sciaini and others 2018). Although we set this range in the number of cells, we communicate these values by calculating the area of a circle with a radius equal to the specified variogram range and scaling that area as a percentage of the grid area (Figure 2b). For instance, on our 10^6-cell grid, a circle with a radius of 126 cells has an area equal to 5% of the grid area, and we refer to this percentage as the scale of spatial autocorrelation.

After running the simulations across a range of scales of spatial autocorrelation, we verified that the mean reburn area across replicates remained equal to the value determined analytically Eq. (1). However, as we increased the scale of spatial autocorrelation (that is, as the size of simulated fires increases), the variation in reburn area across replicates also increased (Figure 2b). Thus, before we could compare the observed reburn area to the distribution of simulated reburn areas, we had to calibrate the scale of spatial autocorrelation to best match the simulated to the observed patch-size distribution. We used the 'patches' function of the R 'terra' package (Hijmans and others 2024) to identify patches of contiguous burned cells (searching in eight directions) for each year of the observed record and each year of the simulation. Then, we compiled patch sizes across the 33-year record to construct the full patch-size distribution (Figure 2c).

To determine the appropriate scale of spatial autocorrelation, we ran the model for 500 replicates each at various scales of spatial autocorrelation, and we adjusted the autocorrelation parameter iteratively to improve the correspondence between the simulated and observed patch-size distributions (Figure 2c). We prioritized matching the sizes of the larger patches that comprise the vast majority of the area burned over time. To facilitate this comparison, we ranked the observed patches and the simulated patches within each replicate from large to small (Moritz and others 2005). Then, we visually compared the observed patch size for a given rank to both the full range and the interquartile range of simulated patch sizes at the respective rank (Figure 2c).

After selecting the scale of autocorrelation that produced the closest visual match to the observed patch sizes, we repeated the simulation for 1000 replicates and conducted a quantitative comparison. First, we calculated the mean patch size for each rank across all simulation replicates (that is, the mean size of the largest patch per replicate, the mean size of the second largest patch per replicate, etc.). Then, we conducted a two-sample Kolmogorov–Smirnov (KS) test using R function 'ks.test' (R Core Team 2025) to assess whether those means and the observed patch sizes came from the same distribution. To prioritize matching the fit to large patches, we conducted the test iteratively, each time including a larger portion of the patch-size distribution. First, we included only the largest patches to the rank that accounted for 10% of the observed area burned over the 33-year analysis. For each subsequent iteration of the KS test, we progressively increased the minimum patch-size rank (reduced the minimum patch size) to include those patches accounting for an additional 10% of the observed area burned.

After calibration, our simulated patch-size distributions closely matched the observed fire-size distributions. When including the patches accounting for 70% of the total area burned over the 33-year analysis, only four of the 27 FRUs had simulated patch-size distributions that differed significantly from the observed distribution, and none differed from the observed patch-size distributions when including patches accounting for 40% of the total area burned (Appendix S2).

Quantifying the Departure from the Null Model

When averaged across 1000 replicates, the mean of the simulated reburn areas was nearly identical to the value determined analytically Eq. (1), and the simulated reburn areas were normally distributed around the analytically-determined value. Therefore, we fit a normal distribution to the simulated reburn values using R function 'pnorm' (R Core Team 2025), parameterized using the analytically-determined null reburn area and the standard deviation of the simulated values.

Using the normal distribution fit to the simulated reburn areas, we calculated the area under the outer tail to provide the p-value for a one-sided test of the probability that the results support a significant fire–vegetation feedback. The outer tail of the distribution represents the tail of the curve that extends farther from the null estimate than the observed reburn area. If the observed reburn area was less than the null value, consistent with a negative fire–vegetation feedback, the area under the lower tail would represent the probability that an area less than the observed reburn area could have reburned under the null model. If the ob-

served reburn area was greater than the null value, the area under the upper tail would provide the probability that an area greater than the observed reburn area could have reburned under the null model, thereby representing the strength of a positive feedback.

Results

The observed reburn area was significantly less ($p < 0.05$) than expected under the null model in 17 of the 27 FRUs (Table 1). When summed over these FRUs, the area affected by reburns was 5,037,611 ha less than expected under the null model, representing a reduction of reburn area by 152,655 ha per year, on average. To place these values in context, 73.6 million ha burned across all FRUs from 1986 to 2018, and the observed reburn area accounts for just 3.8% of the total area burned rather than 10.6%, as expected under the null model. Results for each FRU individually are provided in Appendix S3, including a comparison of simulated and observed patch-size distributions.

To help compare patterns across FRUs, we calculated the fire rotation for each FRU over the analysis period by dividing 33 years by the cumulative proportion of the FRU that burned over that interval (Table 1; Baker, 2009). The observed reburn area was farthest below the null value in the FRUs with the shortest fire rotations (that is, the most fire-prone FRUs), and the difference between observed and null values generally decreased as fire rotations became longer (going clockwise in Figure 3 or from right to left in Figure 4a). The 17 FRUs with significantly less reburn area ($p < 0.05$) than expected under the null model include all 14

Table 1. Comparison of differences between the observed reburn area and that simulated under a null model with no feedbacks among 27 Fire Regime Units (FRUs) of the North American boreal forest

FRU	Area	FR	Reburn area (%)		Reburn area (ha)		Reburn difference (ha)		*p*-value
	(km^2)	(yr)	Null	Obs	Null	Obs	Total	Annual	
27	186,619	60	10.38	3.70	1,936,730	689,991	–1,246,739	–37,780	< 0.001
23/25	147,895	79	6.20	1.27	917,396	188,155	–729,241	–22,098	< 0.001
26	266,737	87	5.22	1.36	1,392,636	363,646	–1,028,990	–31,182	< 0.001
8/9	174,850	100	4.01	1.84	700,274	322,341	–377,933	–11,453	< 0.001
33	74,906	104	3.72	0.38	278,427	28,665	–249,762	–7,569	< 0.001
AK	472,376	129	2.57	1.27	1,213,534	598,136	–615,398	–18,648	< 0.001
17	155,524	147	2.06	1.33	319,978	206,859	–113,119	–3,428	< 0.001
22	92,416	149	1.50	0.46	138,717	42,654	–96,063	–2,911	< 0.001
21	156,292	172	1.48	0.97	231,937	151,027	–80,910	–2,452	0.042
40/41	164,242	179	1.36	0.45	223,205	74,028	–149,177	–4,521	< 0.001
29/31	75,839	182	1.33	0.11	100,714	8,674	–92,040	–2,789	< 0.001
35/38	75,232	186	1.15	0.43	86,818	32,340	–54,478	–1,651	0.014
34	127,982	250	0.75	0.06	96,114	7,987	–88,127	–2,671	< 0.001
10	168,001	262	0.63	0.25	105,505	41,621	–63,884	–1,936	0.006
45	81,301	283	0.56	0.39	45,122	31,851	–13,271	–402	0.164
28	79,993	296	0.51	0.32	41,116	25,957	–15,159	–459	0.205
18	140,760	388	0.32	0.33	45,043	46,279	+ 1,236	+ 37	0.466
11	95,251	406	0.25	0.05	23,432	4,723	–18,709	–567	0.127
16	196,537	475	0.21	0.08	40,683	16,589	–24,094	–730	0.011
6	210,349	492	0.20	0.06	42,070	13,035	–29,035	–880	0.003
5	105,045	683	0.06	0.11	9,559	11,770	+ 2,211	+ 67	0.395
32	124,429	751	0.08	0.13	10,203	16,674	+ 6,471	+ 196	0.143
13/15	107,028	915	0.06	0.06	6,101	6,843	+ 742	+ 22	0.426
14	226,723	2,031	0.01	0.01	2,721	2,461	–260	–8	0.466
58	63,771	2,268	0.01	0.03	574	1,953	+ 1,379	+ 42	0.027
1	96,281	3,216	0.00	0.00	193	0	–193	–6	0.340
7	126,868	3,313	0.00	0.00	507	91	–416	–13	0.304

The FRUs are listed in order of increasing fire rotation (FR), as calculated based on the total area burned between 1986 and 2018. The reburn area is represented as the percentage of the FRU area and in hectares. The difference in observed reburn area and that estimated under the null model are presented as the total difference over the 33-year analysis period and the mean annual difference. The p-value was calculated as the area under the outer tail of the normal curve fit to the output of 1000 simulation replicates.

FRUs with fire rotations ≤ 262 years, plus three with longer fire rotations (Table 1). The finding that a 33-year analysis window was long enough to detect a statistically significant reduction in reburn

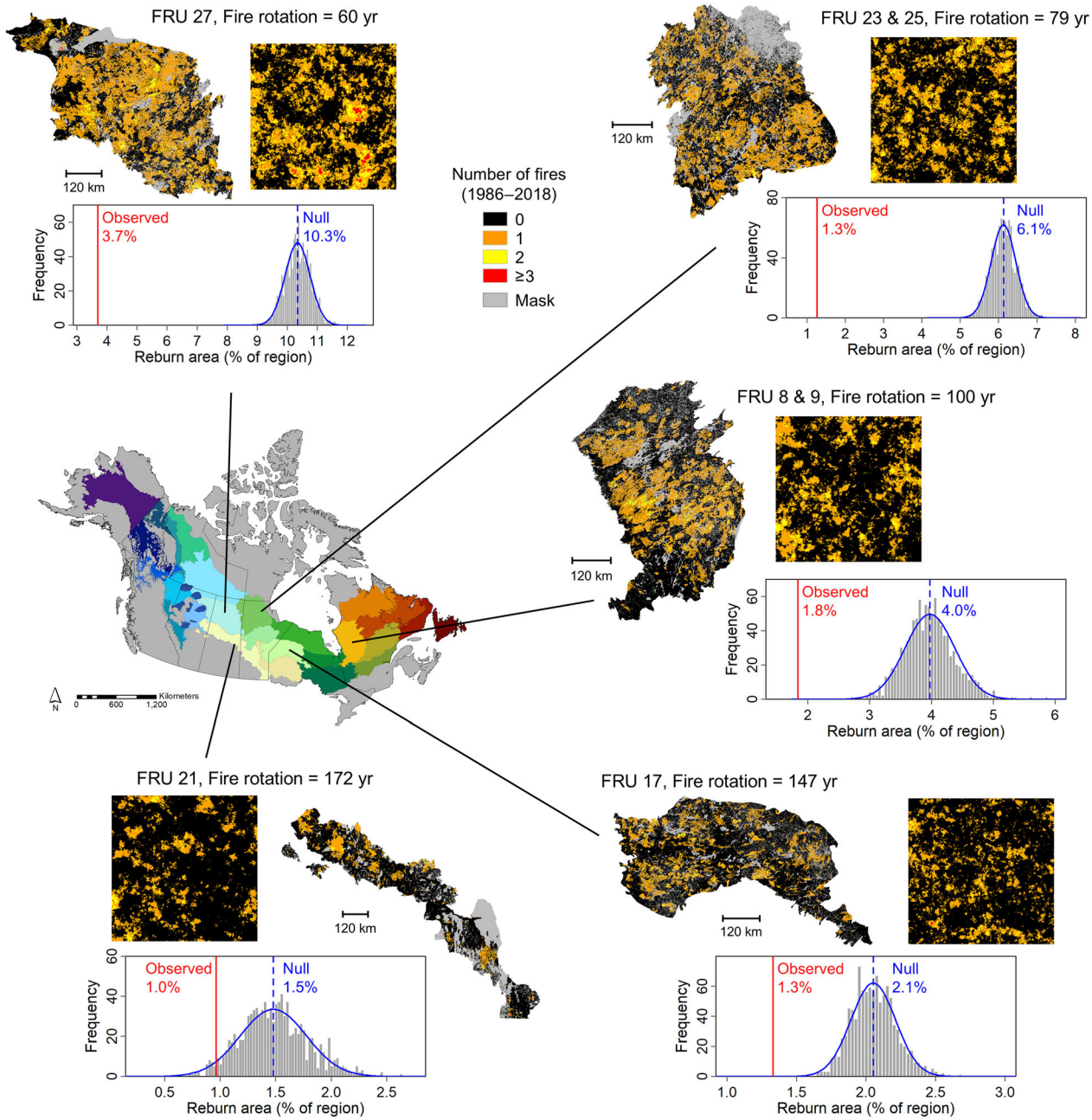

Figure 3. Comparison of the observed reburn extent to that expected under the null model for five selected FRUs across the North American boreal forest. The selected FRUs are arranged in order of increasing fire rotation going clockwise from upper left. For each FRU, we depict the area observed to have burned a given number of times between 1986 and 2018 and the output of one replicate of the simulation with the fire-size distribution calibrated to approximate the observed fire-size distribution. Then, we compared the observed reburn area to the results of 1000 simulation replicates per FRU, where the vertical blue dashed line represents the null reburn area calculated following Eq. 1, and gray bars represent the distribution of reburn areas produced across the 1000 replicates. The solid blue curve is a normal density function fit to that distribution. The statistical significance of the departure from the null model was calculated as the area under the outer tail of the distribution. Complete results for all 27 FRUs are provided in Appendix S3, including a map of the observed fire extent, a time series of annual area burned, maps produced by two simulation replicates, and a comparison of the observed and simulated patch-size distribution and the reburn area results after 1000 replicates.

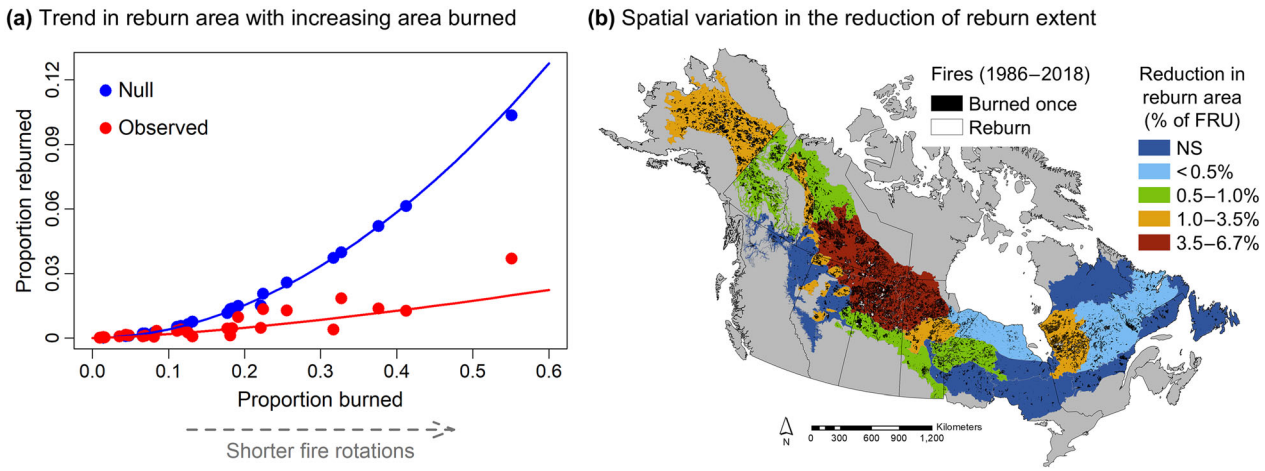

Figure 4. Variation in the reduction in reburn area from 1986 to 2018 across the North American boreal forest. In **a** trends in the null and observed proportion of the FRU that reburned are plotted as a function of the cumulative proportion of the FRU that burned over the analysis period. The proportion burned on the x-axis was calculated as 33 years divided by the fire rotation (provided in Table 1). Spatial variation in the reduction of reburn area relative to the null model is shown in panel, **b** where the magnitude of reduction is shown as the percentage of the FRU area (NS indicates FRUs where the observed reburn area was not significantly lower than expected under the null model). Although points for all FRUs are plotted in, **a** the curves were fit using only the FRUs for which the observed reburn extent was significantly lower than expected under the null model. We modeled the proportion of the FRU that reburned (r) within the analysis window as a power function of the cumulative proportion of the FRU that burned, **b** within the analysis window. The resulting equations are $r = 0.342b^{1.929}$ ($R^2 = 0.998$, $p < 0.001$) for the null model and $r = 0.046b^{1.399}$ ($R^2 = 0.719$, $p < 0.001$) for the observed data. Note that the x-axis value for each FRU corresponds to the proportion of its fire rotation included within the 33-year analysis window.

area in each of these FRUs (and highly signification reductions, $p < 0.001$, in 11 of them) illustrates the strength of the negative feedback.

The 10 FRUs where the observed reburn area was not significantly different from the null model ($p > 0.05$) were among the least fire-prone FRUs, each with a fire rotation ≥ 283 years (Table 1). Failure to reject the null model in these FRUs could indicate that fire–vegetation feedbacks were weak or absent. Alternatively, with so little fire, a 33-year analysis may have been too short to include opportunities for fires to encroach upon the perimeters of other recently burned areas, leaving little chance for feedbacks to play out (Appendix S3).

The observed reburn area was significantly greater than the null value in only one FRU (FRU 58, $p = 0.027$), but only by 1379 ha (Table 1). This was one of the least fire-prone FRUs (fire rotation > 2000 years), and 77% of the reburn area occurred when a portion of a single fire from 1990 was reburned by another fire in 2018, at close to the longest reburn interval in our analysis. A single reburn event was sufficient to drive a statistically significant increase relative to the null model, but with so little fire in the FRU, this result should not imply that this difference would hold when viewed over a longer analysis window.

By comparing observed to null reburn extents across FRUs with such a wide range of fire rotations, we gained insight into whether the negative feedback (that is, the resistance to reburning) is likely to persist in the face of climate change-driven increases in wildfire activity. Under the null model, we demonstrated a clear trend whereby the proportion of an FRU expected to reburn increases as the proportion of the FRU that burned over the analysis period increases (Figure 4a). The observed extent of reburns also increased with increasing area burned across the FRUs, but at a much slower rate. Thus, for the three most fire-prone FRUs (FRUs 23/25, 26, and 27 of north-central Canada), we would have expected an additional 3.9–6.7% of the land area (just over 3 million hectares; Table 1) to have burned more than once between 1986 and 2018 in the absence of a feedback (Figure 2b).

If the capacity to resist reburning is similar across FRUs (that is, if the feedback mechanisms are similar across the NAB), but the difference from the null model across FRUs was driven largely differences in the opportunities for those feedback mechanisms to play out (that is, opportunities for fires to encounter a recently burned area), the

trend across FRUs in Figure 4a would represent the likely trend within an FRU in response to increasing wildfire activity. As annual area burned increases, points would shift to the right along the x-axis, and the null and expected curves illustrate the expectations for the corresponding increase in reburn area with and without feedbacks.

Discussion

We found strong and widespread resistance to reburning (that is, a negative fire–vegetation feedback) across the NAB, which led to a 5 Mha reduction in reburn extent over 33 years compared to the null expectation without a feedback (Figs. 3 and 4). The feedback was strong enough that a 33-year fire record was sufficient to find a statistically significant reduction in reburn area in each FRU with a contemporary fire rotation ≤ 262 years (Table 1). The reduction in reburn extent was strongest in the FRUs with the shortest fire rotation (down to 60 years in FRU 27, northern Saskatchewan; Table 1 and Figure 3), illustrating that the effects of the negative feedback were greatest where there were the most opportunities for the feedbacks to play out (that is, where fires spread into recently burned areas). Thus, the reduction in reburn extent was strong in central and western Canada and Alaska, excluding the less fire-prone areas near the foothills of the Rocky Mountains. In eastern Canada, only the areas east of the Hudson and James Bays in northwestern Québec (FRU 8/9) had a strong reduction in reburn extent relative to the null model, but with the fourth shortest fire rotation overall, this FRU was by far the most fire-prone part of eastern Canada (Table 1, Figure 4b).

Our finding of a strong negative feedback in the most fire-prone FRUs (that is, those with the shortest fire rotations) suggests the resistance to reburning will likely continue to limit wildfire activity across much of the NAB, even as the climate continues to warm and become more conducive to fire, assuming similar feedback mechanisms play out across the other FRUs. However, if climate and severe fire weather were to increasingly override the feedback (Buma and others 2022; Whitman and others 2024), or if conifer forests were increasingly converted to either less-flammable deciduous species (Johnstone and others 2011; Kelly and others 2013) or more fire-prone grasslands (Stralberg and others 2018), our analyses will provide a baseline from which to identify the change.

Influence of Feedbacks on Boreal Fire Regimes

Resistance to reburning at short intervals has long influenced fire regimes across the NAB. For instance, tree-ring fire scars and establishment dates along a 190-km-long transect in northern Québec suggest that fire frequency increased over time since fire, with stands < 50 years being less fire prone than older stands (Héon and others 2014). After expanding the transect to 320 km, stands < 50 years old remained resistant to burning, and this resistance was found to reduce the burn rate to about 40% of that expected without the feedback (Erni and others 2017). This resistance to reburning is consistent with gradual fuel accumulation following severe fire (Johnston and others 2015; Thompson and others 2017; Walker and others 2020).

Increasing wildfire activity has potential to strengthen the feedback in northwestern portions of the NAB, where extensive fires over the last couple of decades have driven a shift toward increasing cover of broadleaf deciduous trees that are less flammable than conifers (Beck and others 2011; Mann and others 2012). This shift could become more pronounced with further climate-driven increases wildfire activity (Baltzer and others 2021; Walker and others 2023) because once deciduous trees become established in former conifer-dominated stands, subsequent fires tend to perpetuate or increase their dominance (Hansen and others 2021; Hayes and Buma 2021). The low flammability of deciduous species may lead to a particularly strong negative feedback (Bernier and others 2016; Cuming, 2001; Hély and others 2000), which could offset a portion of the increases in wildfire activity and associated carbon emissions otherwise expected in a warming climate (Terrier and others 2013; Foster and others 2022).

Although shifts toward increasing deciduous cover were found to have dampened fire activity when the climate was otherwise conducive to widespread fire in the paleoecological record in both the western and eastern NAB (Girardin and others 2013; Kelly and others 2013; Hoecker and Higuera 2019), recent fire-driven increases in deciduous cover have been limited primarily to the northwestern NAB (Johnstone and others 2010, 2020; Mack and others 2021). In the eastern NAB, forest harvesting has contributed to the expansion of aspen cover (Marchais and others 2022), but fire-driven reductions in black spruce dominance currently favor replacement by jack pine (Baltzer and others 2021). However, fire intervals < 30 years

could eventually limit post-fire jack pine regeneration due to the immaturity risk (that is, insufficient time for adequate seed production; Splawinski and others 2019, Augustin and others 2022).

Despite evidence of the negative feedback moderating the effects of climate on area burned in the paleoecological record, recent fire extent may be exceeding that found over the past several millennia (Kelly and others 2013). Studies of contemporary reburns have found that the negative feedback was strongest within the first decade following fire, followed by a gradual weakening to the point where it could more easily be overcome by severe fire weather by 20 years following fire (Buma and others 2022; Whitman and others 2024). Days of extensive fire growth under severe fire weather have the greatest potential to override the negative feedback. These days are increasingly recognized as important drivers of total area burned (Balik and others 2024), and they are likely to become more common under future climate (Jain and others 2022). However, our finding that the departure from the null model was strongest in the most fire-prone FRUs (that is, those with the shortest fire rotations; Table 1), suggests potential for the feedback to continue to limit wildfire activity.

Fire patterns during some of the most extensive recent fire years, including the record-breaking fire season of 2023 (Jain and others 2024), support our interpretation that the negative feedback will continue to moderate future fire patterns, even if the feedback is weakened to some degree. For example, 2.5 Mha burned across the eastern Northwest Territories in 2023 (FRU 26, the third most fire-prone FRU; Table 1). Just over 90% of the burned area within the FRU had no recent fire, despite 38% of the FRU having been burned at least once within the previous 33 years (equivalent to the length of our analysis). More than 2 Mha also burned across this FRU in 2014, when the province had been under prolonged drought since the previous fall, with precipitation 30% below normal and temperatures 1.5–2.5°C above normal through June and July (Kochtubajda and others 2019). Although 24% of the FRU had burned at least once over the preceding 33 years, this recently burned area comprised only 3.3% of the area that burned in 2014. Even in such a severe fire season, more than 96% of the fire extent was in areas with no recent fire.

Our analyses could be repeated in another decade or two to test for a weakening of the feedback. We expect to see increasing wildfire activity as the climate continues to warm and severe fire weather becomes more common (Boulanger and others 2024; Kirchmeier-Young and others 2024). Increasing wildfire activity would lead to an increase in reburn area as recently burned areas cover a greater proportion of the landscape (that is, a larger area will be available to reburn), and there are more opportunities for fires to interact with that recently burned area. However, such changes would not necessarily indicate a weakening of the feedback. As climate-driven increases in wildfire activity lead to shorter fire rotations, FRUs would shift to the right along the *x*-axis of Figure 4a, and we would expect a corresponding increase in reburn extent. Such an increase would not represent a weakening of the feedback unless the slope of the observed curve becomes steeper, or if individual FRUs became strong outliers above the curve.

Strengths and Limitations

One of the main strengths of our modeling approach is the ability to calibrate and apply this approach using data readily available in many regions globally. The inputs were limited to fire perimeters spanning a couple of decades (for example, spanning the Landsat record; Eidenshink and others 2007; Hall and others 2020) and a land-cover dataset that can be used to mask out non-burnable parts of the landscape. In addition, the model should be applied to regions where the fire regime is relatively homogenous—in our case, the FRUs of Erni et al. (2020)—to allow for the null assumption that in each year, all of the landscape would be equally likely to burn in the absence of a fire–vegetation feedback.

After acquiring a time series of annual area burned for the study region, the analytical model can quickly be applied to quantify the degree to which the observed reburn area departs from the null value with no need for further calibration or running a time-consuming simulation. The ability to formulate this process mathematically Eq. (1) strengthens our understanding of how reburn dynamics would play out in a system with top-down variation in annual area burned but no bottom-up feedbacks. The spatial simulation then corroborates the results of the analytical model and provides confidence intervals needed to determine if the difference between null and observed reburn extents is statistically significant. Comparing the two modeling approaches demonstrates how increasing fire size drives wider variation around the null reburn area. This modeling approach could easily be expanded to compare results across diverse regions. For instance, adding results from

regions with a positive fire–vegetation feedback (Kitzberger and others 2016; Lindenmayer and others 2022; Zylstra and others 2023) to Figure 4a would be expected to produce data points above the curve representing the null model.

Despite the relative ease of running the model, there were three main limitations. First, our modeling approach uses the observed time series of annual area burned to calculate the expected reburn area under the null model. However, in the case of a negative feedback, resistance to reburning would limit not just which areas burn, but also the total area burned per year (Boulanger and others 2017; Marchal and others 2019; Gaboriau and others 2023). Without a negative feedback, the total area burned during extensive fire years like 2023 would have been even larger than observed, but our null model does not estimate this additional burned area. Instead, our null model works on the assumption that the annual area burned is driven by top-down processes (that is, climate/weather), and a bottom-up fire–vegetation feedback may influence which parts of the landscape burn each year.

Because our null model does not incorporate an estimate of the additional area that would have burned each year without a negative feedback, our finding that the observed reburn area across the NAB was just over 5 Mha less than expected under the null model from 1986 to 2018 (Table 1) should be viewed as a conservative estimate. The potential for the feedback to contribute to an even greater reduction in reburn area is important to consider given the potential for reburns to substantially alter the trajectory and rate of post-fire vegetation development (Whitman and others 2019; Hayes and Buma 2021) and soil carbon storage (Walker and others 2019).

The second main limitation is that our modeling approach does not account for variation in the strength of the feedback over timescales shorter than the full analysis period (33 years in our case) or account for changes in the feedback as the number of reburns increases. For instance, in boreal forests, the resistance to reburning may be strongest during the first decade or two after fire and then weaken with increasing time since fire (Buma and others 2022; Whitman and others 2024). Because our null model does not account for variation in the strength of the feedback within the analysis period (33 years), our results represent a time-averaged effect of the feedback that could potentially underestimate the strength of the feedback at short intervals ($<$ 10–20 years) and overestimate the effect at longer intervals (up to 33 years). Also, progressive increases in deciduous tree cover over successive reburns (Hayes and Buma 2021) could alter the strength of the feedback in ways not addressed by our null model.

The second limitation could be important if we were to expand our analysis over a period much longer than the duration of the negative feedback or if areas that burned three or more times within the analysis period were common across the study region. However, the slow fuel accumulation after fire in the NAB, combined with the potential for cover-type shifts from conifer to less-flammable deciduous species, makes it likely that at least some resistance to reburning would persist throughout the 33-year analysis window (Héon and others 2014; Thompson and others 2017). Also, areas that burned three or more times over the analysis period accounted for $<$ 2% of the total reburn area in 21 of the 27 FRUs.

Finally, our null model required the assumption that fire regimes are spatially homogeneous within the unmasked portion of each FRU. This assumption could be a problem because distance to waterbodies or the amount of water surrounding a given site may reduce the probability of burning during a particular event (Nielsen and others 2016). However, when considered over decades, the lack of burning during a particular event permits the buildup of fuel that eventually makes sites more fire-prone (Bernier and others 2016). This was the case for the 2013 Eastmain Fire of northern Québec, which burned intensely through a large area of mature conifer forest ($>$ 100 years old) that had previously been protected from fire by lakes and wetlands (Erni et al. 2017). Also, if certain areas were less likely to burn due to topographic protection from fire, but our null model treats all unmasked areas as equally likely to burn, this difference would lead us to find a weaker negative feedback. Because our model uses the observed annual area burned, topographic protection from fire would concentrate this burned area on a smaller portion of the landscape, leading to a greater likelihood of reburning than in our null model.

Conclusions

Resistance to reburning at short intervals has long influenced fire regimes across the NAB. In the past, this resistance has dampened the effects of fire-conducive climate on wildfire extent (Hoecker and Higuera 2019; Gaboriau and others 2023). However, with wildfire extent increasing to unprecedented levels (Kelly and others 2013; Boulanger

and others 2024; Jain and others 2024), it remains uncertain whether the negative feedback will continue to limit future increases in wildfire extent (Buma and others 2022). We evaluated the strength of the negative feedback over recent decades and found it was strong, leading to a conservative estimate of more than 5 Mha less reburn area over 33 years than would be expected in the absence of a feedback.

Our finding that the feedback was strong in the most fire-prone FRUs implies that the resistance to reburning will continue to limit reburn extent, and thus, annual area burned and carbon emissions, even in a warmer, more fire-conducive climate. These results corroborate findings from other approaches to model future fire regimes while accounting for fire–climate–vegetation interactions (Girardin and others 2013; Boulanger and others 2017; Marchal and others 2019; Foster and others 2022). However, uncertainty remains regarding the degree to which a warming climate and severe fire weather will override the feedback or whether the expansion of less-flammable deciduous species could strengthen, or at least, maintain the feedback in the face of a warming climate. Our results provide a sound baseline for identifying any change in the fire–vegetation feedback, and our modeling approach provides a practical method for comparing the direction and strength of the feedback across diverse regions.

ACKNOWLEDGEMENTS

We thank Justin Beckers for his assistance in improving the R code for our simulation model and Emma Sherwood for compiling summary fire regime statistics for the FRUs. The motivation for the analytical part of the model was stimulated by conversations with Enrique Thomann. This work was funded in part by a grant from the Canadian Safety and Security Program (CSSP-2018-TI-2406).

FUNDING

Canadian Safety and Security Program, CSSP-2018-TI-2406.

OPEN ACCESS

DATA AVAILABILITY

The fire perimeters used for the analyses are available in public repositories: the National Burned Area Composite (NBAC; Hall and others 2020; https://cwfis.cfs.nrcan.gc.ca/datamart/metadata/nbac) for Canada and the Monitoring Trends in Burn Severity project (MTBS; Eidenshink and others 2007; https://www.mtbs.gov/) for Alaska. The equation for the analytical part of our model is provided in Eq. 1. Scripts for the analytical and simulation models have been posted to an archive available to the public on Zenodo (https://doi.org/10.5281/zenodo.15678656).

REFERENCES

Abatzoglou JT, Battisti DS, Williams AP, Hansen WD, Harvey BJ, Kolden CA. 2021. Projected increases in western US forest fire despite growing fuel constraints. Communications Earth & Environment 2:1–8.

Archibald S, Lehmann CER, Belcher CM, Bond WJ, Bradstock RA, Daniau A-L, Dexter KG, Forrestel EJ, Greve M, He T, Higgins SI, Hoffmann WA, Lamont BB, McGlinn DJ, Moncrieff GR, Osborne CP, Pausas JG, Price O, Ripley BS, Rogers BM, Schwilk DW, Simon MF, Turetsky MR, der Werf GRV, Zanne AE. 2018. Biological and geophysical feedbacks with fire in the Earth system. Environmental Research Letters 13:033003.

Augustin F, Girardin MP, Terrier A, Grondin P, Lambert M-C, Leduc A, Bergeron Y. 2022. Projected changes in fire activity and severity feedback in the spruce–feather moss forest of western Quebec, Canada. Trees, Forests and People 8:100229.

Baker WL. 2009. Fire ecology in Rocky Mountain landscapes. Washington, DC: Island Press.

Balik JA, Coop JD, Krawchuk MA, Naficy CE, Parisien M-A, Parks SA, Stevens-Rumann CS, Whitman E. 2024. Biogeographic patterns of daily wildfire spread and extremes across North America. Frontiers in Forests and Global Change 7.

Baltzer JL, Day NJ, Walker XJ, Greene D, Mack MC, Alexander HD, Arseneault D, Barnes J, Bergeron Y, Boucher Y, Bourgeau-Chavez L, Brown CD, Carrière S, Howard BK, Gauthier S, Parisien M-A, Reid KA, Rogers BM, Roland C, Sirois L, Stehn S, Thompson DK, Turetsky MR, Veraverbeke S, Whitman E, Yang J, Johnstone JF. 2021. Increasing fire and the

decline of fire adapted black spruce in the boreal forest. Proceedings of the National Academy of Sciences 118:e2024872118.

Beaudoin A, Bernier PY, Guindon L, Villemaire P, Guo XJ, Stinson G, Bergeron T, Magnussen S, Hall RJ. 2014. Mapping attributes of Canada's forests at moderate resolution through kNN and MODIS imagery. Canadian Journal of Forest Research 44:521–532.

Beck PSA, Goetz SJ, Mack MC, Alexander HD, Jin Y, Randerson JT, Loranty MM. 2011. The impacts and implications of an intensifying fire regime on Alaskan boreal forest composition and albedo. Global Change Biology 17:2853–2866.

Bernier PY, Gauthier S, Jean P-O, Manka F, Boulanger Y, Beaudoin A, Guindon L. 2016. Mapping local effects of forest properties on fire risk across Canada. Forests 7:157.

Boulanger Y, Girardin M, Bernier PY, Gauthier S, Beaudoin A, Guindon L. 2017. Changes in mean forest age in Canada's forests could limit future increases in area burned but compromise potential harvestable conifer volumes. Canadian Journal of Forest Research 47:755–764.

Boulanger Y, Arseneault D, Bélisle AC, Bergeron Y, Boucher J, Boucher Y, Danneyrolles V, Erni S, Gachon P, Girardin MP, Grant E, Grondin P, Jetté J-P, Labadie G, Leblond M, Leduc A, Puigdevall JP, St-Laurent M-H, Tremblay J, Waldron K. 2024. The 2023 wildfire season in Québec: an overview of extreme conditions, impacts, lessons learned and considerations for the future. Canadian Journal of Forrest Research 55:1–21.

Brandt JP. 2009. The extent of the North American boreal zone. Environ Rev 17:101–161.

Brandt JP, Flannigan MD, Maynard DG, Thompson ID, Volney WJA. 2013. An introduction to Canada's boreal zone: ecosystem processes, health, sustainability, and environmental issues. Environmental Reviews 21:207–226.

Buma B, Weiss S, Hayes K, Lucash M. 2020. Wildland fire reburning trends across the US West suggest only short-term negative feedback and differing climatic effects. Environmental Research Letters 15:034026.

Buma B, Hayes K, Weiss S, Lucash M. 2022. Short-interval fires increasing in the Alaskan boreal forest as fire self-regulation decays across forest types. Scientific Reports 12:4901.

Burrell AL, Sun Q, Baxter R, Kukavskaya EA, Zhila S, Shestakova T, Rogers BM, Kaduk J, Barrett K. 2022. Climate change, fire return intervals and the growing risk of permanent forest loss in boreal Eurasia. Science of the Total Environment 831:154885.

Cuming SG. 2001. Forest type and wildfire in the Alberta boreal mixedwood: What do fires burn? Ecol Appl 11:97–110.

de Groot WJ, Cantin AS, Flannigan MD, Soja AJ, Gowman LM, Newbery A. 2013. A comparison of Canadian and Russian boreal forest fire regimes. Forest Ecology and Management 294:23–34.

Eidenshink J, Schwind B, Brewer K, Zhu Z-L, Quayle B, Howard S. 2007. A Project for Monitoring Trends in Burn Severity. Fire Ecology 3:3–21.

Environmental Protection Agency. 2013. Level III Ecoregions of the Continental United States. https://www.epa.gov/eco-research/level-iii-and-iv-ecoregions-continental-united-states.

Erni S, Arseneault D, Parisien M-A, Bégin Y. 2017. Spatial and temporal dimensions of fire activity in the fire-prone eastern Canadian taiga. Global Change Biology 23:1152–1166.

Erni S, Wang X, Taylor S, Boulanger Y, Swystun T, Flannigan M, Parisien M-A. 2020. Developing a two-level fire regime zonation system for Canada. Canadian Journal of Forest Research 50:259–273.

Foster AC, Shuman JK, Rogers BM, Walker XJ, Mack MC, Bourgeau-Chavez LL, Veraverbeke S, Goetz SJ. 2022. Bottom-up drivers of future fire regimes in western boreal North America. Environmental Research Letters 17:025006.

Gaboriau DM, Chaste É, Girardin MP, Asselin H, Ali AA, Bergeron Y, Hély C. 2023. Interactions within the climate-vegetation-fire nexus may transform 21st century boreal forests in northwestern Canada. Science 26.

Gardner RH. 2017. Characterizing Categorical Map Patterns Using Neutral Landscape Models. In: Gergel SE, Turner MG, Eds. Learning Landscape Ecology: A Practical Guide to Concepts and Techniques, . New York: Springer. pp 83–103.

Girardin MP, Ali AA, Carcaillet C, Blarquez O, Hély C, Terrier A, Genries A, Bergeron Y. 2013. Vegetation limits the impact of a warm climate on boreal wildfires. New Phytologist 199:1001–1011.

Hall RJ, Skakun RS, Metsaranta JM, Landry R, Fraser RH, Raymond D, Gartrell M, Decker V, Little J. 2020. Generating annual estimates of forest fire disturbance in Canada: The National Burned Area Composite. International Journal of Wildland Fire 29:878–891.

Hanes CC, Wang X, Jain P, Parisien M-A, Little JM, Flannigan MD. 2019. Fire-regime changes in Canada over the last half century. Canadian Journal of Forest Research 49:256–269.

Hansen WD, Fitzsimmons R, Olnes J, Williams AP. 2021. An alternate vegetation type proves resilient and persists for decades following forest conversion in the North American boreal biome. Journal of Ecology 109:85–98.

Hart SJ, Henkelman J, McLoughlin PD, Nielsen SE, Truchon-Savard A, Johnstone JF. 2019. Examining forest resilience to changing fire frequency in a fire-prone region of boreal forest. Global Change Biology 25:869–884.

Hayes K, Buma B. 2021. Effects of short-interval disturbances continue to accumulate, overwhelming variability in local resilience. Ecosphere 12:e03379.

Hély C, Bergeron Y, Flannigan MD. 2000. Effects of stand composition on fire hazard in mixed-wood Canadian boreal forest. J Veg Sci 11:813–824.

Héon J, Arseneault D, Parisien M-A. 2014. Resistance of the boreal forest to high burn rates. Proceedings of the National Academy of Sciences 111:13888–13893.

Hijmans RJ, Bivand R, Dyba K, Pebesma E, Sumner MD. 2024. terra: Spatial Data Analysis. https://cran.r-project.org/web/packages/terra/index.html.

Hoecker TJ, Higuera PE. 2019. Forest succession and climate variability interacted to control fire activity over the last four centuries in an Alaskan boreal landscape. Landscape Ecology 34:227–241.

Hong Y. 2013. On computing the distribution function for the Poisson binomial distribution. Computational Statistics & Data Analysis 59:41–51.

Jain P, Castellanos-Acuna D, Coogan SCP, Abatzoglou JT, Flannigan MD. 2022. Observed increases in extreme fire weather driven by atmospheric humidity and temperature. Nature Climate Change 12:63–70.

Jain P, Barber QE, Taylor SW, Whitman E, Castellanos Acuna D, Boulanger Y, Chavardes RS, Chen J, Englefield P, Flannigan M, Girardin MP, Hanes CC, Little J, Morrison K, Skakun RS, Thompson DK, Wang X, Parisien M-A. 2024. Drivers and

impacts of the record-breaking 2023 wildfire season in Canada. Nature Communications 15:6764.

Johnston DC, Turetsky MR, Benscoter BW, Wotton BM. 2015. Fuel load, structure, and potential fire behaviour in black spruce bogs. Canadian Journal of Forest Research 45:888–899.

Johnstone JF, Hollingsworth TN, Chapin FS, Mack MC. 2010. Changes in fire regime break the legacy lock on successional trajectories in Alaskan boreal forest. Global Change Biology 16:1281–1295.

Johnstone JF, Rupp TS, Olson M, Verbyla D. 2011. Modeling impacts of fire severity on successional trajectories and future fire behavior in Alaskan boreal forests. Landscape Ecology 26:487–500.

Johnstone JF, Celis G, Chapin FS, Hollingsworth TN, Jean M, Mack MC. 2020. Factors shaping alternate successional trajectories in burned black spruce forests of Alaska. Ecosphere 11:e03129.

Kelly R, Chipman ML, Higuera PE, Stefanova I, Brubaker LB, Hu FS. 2013. Recent burning of boreal forests exceeds fire regime limits of the past 10,000 years. Proceedings of the National Academy of Sciences 110:13055–13060.

Kirchmeier-Young MC, Malinina E, Barber QE, Garcia Perdomo K, Curasi SR, Liang Y, Jain P, Gillett NP, Parisien M-A, Cannon AJ, Lima AR, Arora VK, Boulanger Y, Melton JR, Van Vliet L, Zhang X. 2024. Human driven climate change increased the likelihood of the 2023 record area burned in Canada. NPJ Climatic and Atmospheric Science 7:1–12.

Kitzberger T, Perry GLW, Paritsis J, Gowda JH, Tepley AJ, Holz A, Veblen TT. 2016. Fire–vegetation feedbacks and alternative states: common mechanisms of temperate forest vulnerability to fire in southern South America and New Zealand. New Zealand Journal of Botany 54:247–272.

Kochtubajda B, Steward RE, Flannigan MD, Bonsal BR, Cuell C, Mooney CJ. 2019. An assessment of surface and atmospheric conditions assoiated with the extreme 2014 wildfire season in Canada's Northwest Territories. Atmosphere-Ocean 57:73–90.

Lindenmayer DB, Bowd EJ, Taylor C, Likens GE. 2022. The interactions among fire, logging, and climate change have sprung a landscape trap in Victoria's montane ash forests. Plant Ecology 223:733–749.

Mack MC, Walker XJ, Johnstone JF, Alexander HD, Melvin AM, Jean M, Miller SN. 2021. Carbon loss from boreal forest wildfires offset by increased dominance of deciduous trees. Science 372:280–283.

Mann DH, Scott Rupp T, Olson MA, Duffy PA. 2012. Is Alaska's boreal forest now crossing a major ecological threshold? Arctic, Antarctic, and Alpine Research 44:319–331.

Marchais A, Arsenault D, Bergeron Y. 2022. The rapid expansion of *Populus tremuloides* due to anthropogenic disturbances in eastern Canada. Canadian Journal of Forest Research 52:991–1001.

Marchal J, Cumming SG, McIntire EJB. 2019. Turning down the heat: Vegetation feedbacks limit fire regime responses to global warming. Ecosystems 23:204–216.

Massey R, Rogers BM, Berner LT, Cooperdock S, Mack MC, Walker XJ, Goetz SJ. 2023. Forest composition change and biophysical climate feedbacks across boreal North America. Nature Climate Change 13:1368–1375.

Moritz MA, Morais ME, Summerell LA, Carlson JM, Doyle J. 2005. Wildfires, complexity, and highly optimized tolerance. Proceedings of the National Academy of Sciences 102:17912–17917.

Nielsen SE, DeLancey ER, Reinhardt K, Parisien M-A. 2016. Effects of lakes on wildfire activity in the boreal forests of Saskatchewan. Canada. Forests 7:265.

Pan Y, Birdsey RA, Fang J, Houghton R, Kauppi PE, Kurz WA, Phillips OL, Shvidenko A, Lewis SL, Canadell JG, Ciais P, Jackson RB, Pacala SW, McGuire AD, Piao S, Rautiainen A, Sitch S, Hayes D. 2011. A Large and Persistent Carbon Sink in the World's Forests. Science 333:988–993.

Parisien M-A, Barber QE, Flannigan MD, Jain P. 2023. Broadleaf tree phenology and springtime wildfire occurrence in boreal Canada. Global Change Biology 29:6106–6119.

Parks SA, Holsinger LM, Miller C, Nelson CR. 2015. Wildland fire as a self-regulating mechanism: the role of previous burns and weather in limiting fire progression. Ecological Applications 25:1478–1492.

Parks SA, Parisien M-A, Miller C, Holsinger LM, Baggett LS. 2018. Fine-scale spatial climate variation and drought mediate the likelihood of reburning. Ecological Applications 28:573–586.

Phillips CA, Rogers BM, Elder M, Cooperdock S, Moubarak M, Randerson JT, Frumhoff PC. 2022. Escalating carbon emissions from North American boreal forest wildfires and the climate mitigation potential of fire management. Science Advances 8:eabl7161.

R Core Team. 2025. R: A language and environment for statistical computing. Version 4.4.3. https://www.R-project.org/

Rantanen M, Karpechko AY, Lipponen A, Nordling K, Hyvärinen O, Ruosteenoja K, Vihma T, Laaksonen A. 2022. The Arctic has warmed nearly four times faster than the globe since 1979. Communications Earth & Environment 3:1–10.

Rogers BM, Soja AJ, Goulden ML, Randerson JT. 2015. Influence of tree species on continental differences in boreal fires and climate feedbacks. Nature Geoscience 8:228–234.

Ross S. 2010. A First Course in Probability, 8th edn. Upper Saddle River, NJ: Prentice Hall.

Sciaini M, Fritsch M, Scherer C, Simpkins CE. 2018. NLMR and landscapetools: An integrated environment for simulating and modifying neutral landscape models in R. Methods in Ecology and Evolution 9:2240–2248.

Shenoy A, Johnstone JF, Kasischke ES, Kielland K. 2011. Persistent effects of fire severity on early successional forests in interior Alaska. Forest Ecology and Management 261:381–390.

Skakun R, Castilla G, Metsaranta J, Whitman E, Rodrigue S, Little J, Groenewegen K, Coyle M. 2022. Extending the National Burned Area Composite time series of wildfires in Canada. Remote Sensing 14:3050.

Splawinski TB, Cyr D, Gauthier S, Jetté J-P, Bergeron Y. 2019. Analyzing risk of regeneration failure in the managed boreal forest of northwestern Quebec. Canadian Journal of Forest Research 49:680–691.

Stocks BJ, Mason JA, Todd JB, Bosch EM, Wotton BM, Amiro BD, Flannigan MD, Hirsch KG, Logan KA, Martell DL, Skinner WR. 2002. Large forest fires in Canada, 1959–1997. Journal of Geophysical Research: Atmospheres 107:FFR 5–1-FFR 5–12.

Stralberg D, Wang X, Parisien M-A, Robinne F-N, Sólymos P, Mahon CL, Nielsen SE, Bayne EM. 2018. Wildfire-mediated vegetation change in boreal forests of Alberta Canada. Ecosphere 9:e02156.

Terrier A, Girardin MP, Périé C, Legendre P, Bergeron Y. 2013. Potential changes in forest composition could reduce impacts

of climate change on boreal wildfires. Ecological Applications 23:21–35.

Thompson DK, Parisien M-A, Morin J, Millard K, Larsen CPS, Simpson BN. 2017. Fuel accumulation in a high-frequency boreal wildfire regime: from wetland to upland. Canadian Journal of Forest Research 47:957–964.

Tymstra C, Stocks BJ, Cai X, Flannigan MD. 2020. Wildfire management in Canada: Review, challenges and opportunities. Progress in Disaster Science 5:100045.

Walker XJ, Baltzer JL, Cumming SG, Day NJ, Ebert C, Goetz S, Johnstone JF, Potter S, Rogers BM, Schuur EAG, Turetsky MR, Mack MC. 2019. Increasing wildfires threaten historic carbon sink of boreal forest soils. Nature 572:520–523.

Walker XJ, Rogers BM, Veraverbeke S, Johnstone JF, Baltzer JL, Barrett K, Bourgeau-Chavez L, Day NJ, de Groot WJ, Dieleman CM, Goetz S, Hoy E, Jenkins LK, Kane ES, Parisien M-A, Potter S, Schuur EAG, Turetsky M, Whitman E, Mack MC. 2020. Fuel availability not fire weather controls boreal wildfire severity and carbon emissions. Nature Climate Change 10:1130–1136.

Walker XJ, Okano K, Berner LT, Massey R, Goetz SJ, Johnstone JF, Mack MC. 2023. Shifts in Ecological Legacies Support Hysteresis of Stand Type Conversions in Boreal Forests. Ecosystems 26:1796–1805.

Whitman E, Parisien M-A, Thompson DK, Flannigan MD. 2018. Topoedaphic and forest controls on post-fire vegetation assemblies are modified by fire history and burn severity in the northwestern Canadian boreal forest. Forests 9:151.

Whitman E, Parisien M-A, Thompson DK, Flannigan MD. 2019. Short-interval wildfire and drought overwhelm boreal forest resilience. Scientific Reports 9:18796.

Whitman E, Barber QE, Jain P, Parks SA, Guindon L, Thompson DK, Parisien M-A. 2024. A modest increase in fire weather overcomes resistance to fire spread in recently burned boreal forests. Global Change Biology 30:e17363.

Wooster MJ, Zhang YH. 2004. Boreal forest fires burn less intensely in Russia than in North America. Geophysical Research Letters 31.

Zhang X, Flato G, Kirchmeier-Young M, Vincent L, Wan H, Wang X, Rong R, Fyfe J, Li G, Kharin VV. 2019. Changes in Temperature and Precipitation Across Canada. In: Bush E, Lemmen DS, editors. Canada's Changing Climate Report. Ottawa, Ontario, Canada: Government of Canada. pp 112–93.

Zylstra P, Wardell-Johnson G, Falster D, Howe M, McQuoid N, Neville S. 2023. Mechanisms by which growth and succession limit the impact of fire in a south-western Australian forested ecosystem. Functional Ecology 37:1350–1365.